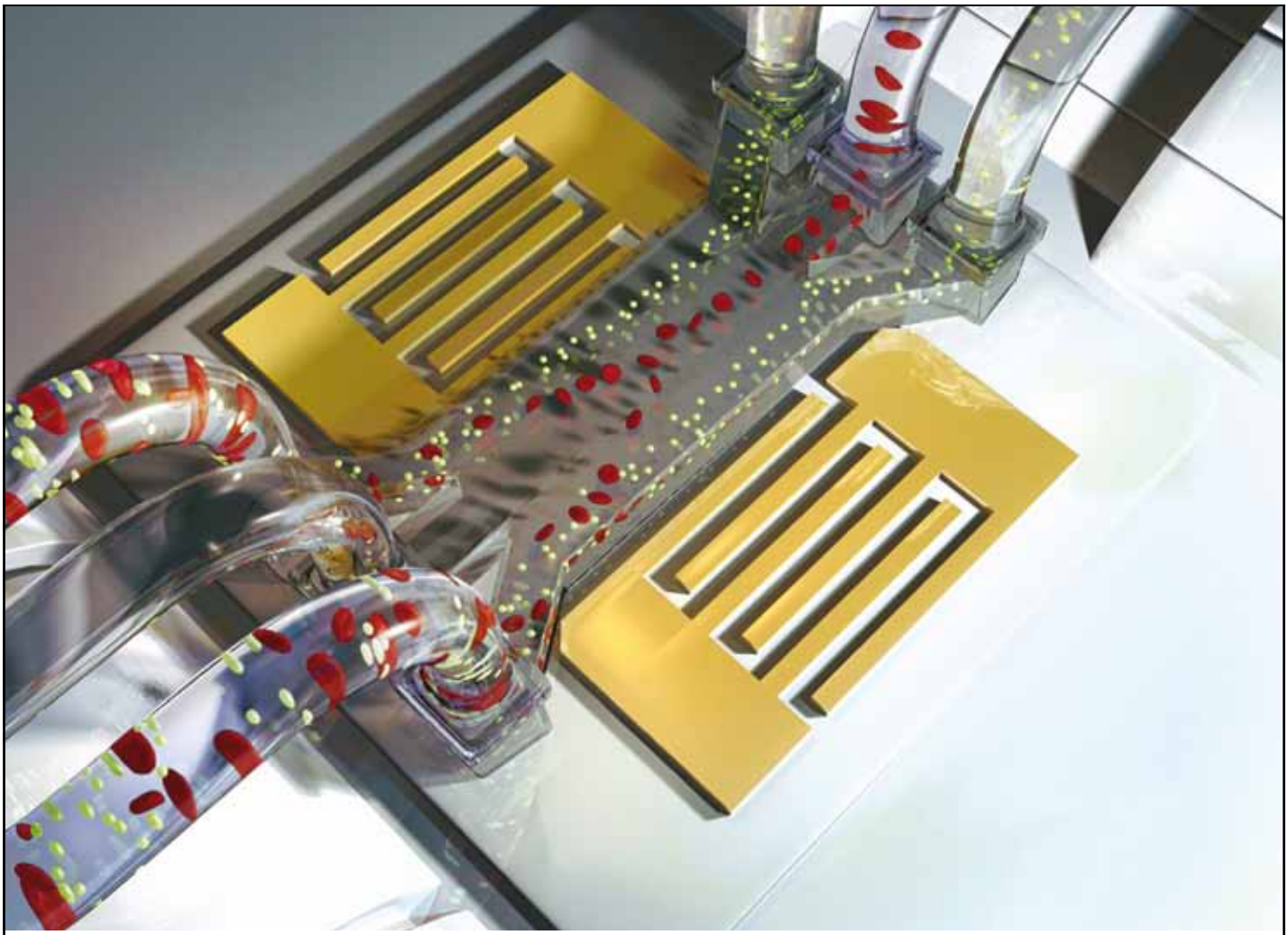

Featuring work from the group of Professor T. J. Huang in the Department of Engineering Science and Mechanics, The Pennsylvania State University, University Park, PA, USA

Title: Continuous particle separation in a microfluidic channel *via* standing surface acoustic waves (SSAW)

"Acoustic tweezers" enable on-chip continuous particle separation through standing surface acoustic wave (SSAW)-induced acoustophoresis in a microfluidic channel.

As featured in:

See Huang *et al.*, *Lab Chip*, 2009, **9**, 3354–3359.

RSC Publishing

www.rsc.org

Registered Charity Number 207890

Continuous particle separation in a microfluidic channel *via* standing surface acoustic waves (SSAW)

Jinjie Shi,†[a] Hua Huang ,†[ab] Zak Stratton,[a] Yiping Huang[b] and Tony Jun Huang*[a]

Received 24th July 2009, Accepted 11th September 2009
First published as an Advance Article on the web 12th October 2009
DOI: 10.1039/b915113c

This work introduces a method of continuous particle separation through standing surface acoustic wave (SSAW)-induced acoustophoresis in a microfluidic channel. Using this SSAW-based method, particles in a continous laminar flow can be separated based on their volume, density and compressibility. In this work, a mixture of particles of equal density but dissimilar volumes was injected into a microchannel through two side inlets, sandwiching a deonized water sheath flow injected through a central inlet. A one-dimensional SSAW generated by two parallel interdigital transducers (IDTs) was established across the channel, with the channel spanning a single SSAW pressure node located at the channel center. Application of the SSAW induced larger axial acoustic forces on the particles of larger volume, repositioning them closer to the wave pressure node at the center of the channel. Thus particles were laterally moved to different regions of the channel cross-section based on particle volume. The particle separation method presented here is simple and versatile, capable of separating virtually all kinds of particles (regardless of charge/polarization or optical properties) with high separation efficiency and low power consumption.

Introduction

Simple and efficient particle separation methods are fundamentally important in biological and chemical analyses such as cancer cell detection, drug screening, and tissue engineering.[1–4] To date, many methods capable of particle separation in microfluidic systems have been demonstrated, including centrifugal,[5–7] magnetic,[8,9] hydrodynamic[10–21] and electrokinetic/dielectrophoretic (DEP)[17,20,22–26] methods. Centrifugal separation is one of the most widely used particle separation methods, using centrifugal force—generated by spinning a sample in a rotating chamber—to separate heavier particles from lighter particles. The magnetic method is operated by first labeling the particles of interest with magnetic materials and then applying an external magnetic field to the sample, thereby separating the labeled particles from the mixture. An additional continuous on-chip separation scheme employs hydrodynamic methods in which properly designed channels (*i.e.*, asymmetric obstacles inside the channel) direct particles of different sizes to different channel outlets. This method permits versatile device design and continuous operation without requiring the input of external forces. However, the device layout and channel obstacles are static, significantly limiting device use by preventing its sorting parameters from being changed. Another example of continuous on-chip particle separation is through dielectrophoresis (DEP), in which an external electric field is used to separate particles with different charge/polarization properties.

Recently developed bulk acoustic wave (BAW)-based acoustophoresis techniques have enabled the separation of microparticles of different sizes and densities in microfluidic channels.[27,28] This approach uses bulky transducers to generate BAWs, which are then coupled into a silicon-based microchannel with a width equal to half the BAW wavelength. The resonance of the BAWs inside the channel results in a standing BAW field with a pressure node at the channel center. Particles injected along the sidewalls of the channel experience axial acoustic forces whose magnitudes depend on the particle size, density, and compressibility. These differing forces reposition the particles with different lateral displacements, thus achieving particle separation.[28] This method is notably advantageous because it requires no pretreatment of the particles and can be applied to virtually all kinds of particles, regardless of optical or charge properties. However, the formation of the standing BAW requires the channel material to possess excellent acoustic reflection properties (*e.g.*, silicon, glass, *etc.*)—properties that the soft polymer materials commonly used in microfluidic applications, such as polydimethylsiloxane (PDMS), do not have.[29] Additionally, the transducer required for BAW generation is bulky, hindering device integration and miniaturization.[30]

In this paper, we report a novel approach to acoustophoresis-based particle separation, using standing surface acoustic waves (SSAW) to continuously separate particles in a microfluidic channel. This method features easy fabrication and handling, low cost, and rapid response time. It consumes substantially less power than the BAW method, maintains high separation efficiency, and can be applied to separate virtually all kinds of particles.

[a]*Department of Engineering Science and Mechanics, The Pennsylvania State University, University Park, PA, 16802, USA. E-mail: junhuang@psu.edu; Fax: +814-865-9974; Tel: +814-863-4209*
[b]*ASIC and System State Key Lab, Department of Microelectronics, Fudan University, Shanghai, 200433, PR China*
† These authors contribute equally to this paper.

Working mechanism

A schematic of the SSAW-based separation device is shown in Fig. 1(a). A pair of interdigital transducers (IDTs) was deposited on a transparent piezoelectric substrate, and a PDMS microchannel (with 3 inlets and 3 outlets) was positioned and bonded between these two IDTs. A mixture solution of dissimilar particles was injected through the side inlets and a sheath flow was injected through the central inlet, forming a laminar flow of three liquid streams. Applying AC signals to the IDTs generated two series of identical-frequency surface acoustic waves (SAWs) which propagated in opposite directions toward the channel. The constructive interference of these two SAWs resulted in a SSAW in the area where the microchannel was bonded.[31] When the SSAW encountered the liquids encapsulated in the microfluidic channel, it generated longitudinal leakage waves, causing pressure fluctuations inside the liquids. These pressure fluctuations resulted in lateral acoustic radiation forces (along the X axis in Fig. 1) on the suspended particles, driving them to either the pressure nodes (minimum pressure amplitude) or antinodes (maximum pressure amplitude), depending on the relative density and compressibility between the particles and the medium.[32–41]

As shown in Fig. 1(b), particles in such a SSAW field experience four types of forces: lateral acoustic force (along the X axis), viscous force (opposite direction of particles' velocity relative to flow stream), gravity force (along the Y axis downward), and buoyant force (along the Y axis upward). Among these forces, the gravity force and buoyant force are almost balanced as they are similar in magnitude but opposite in direction. As a result, the behavior of particles inside the channel can be analyzed by examining the viscous force and the acoustic force. In a SSAW, the primary acoustic force (F_r) and the viscous force (F_v) on a particle can be expressed as:[14,15,42,43]

$$F_r = -\left(\frac{\pi {p_0}^2 V_p \beta_m}{2\lambda}\right)\phi(\beta,\rho)\sin(2kx) \quad (1)$$

$$\phi = \frac{5\rho_p - 2\rho_m}{2\rho_p + \rho_m} - \frac{\beta_p}{\beta_m} \quad (2)$$

$$F_v = -6\pi\eta r v \quad (3)$$

where p_0, V_p, λ, k, x, ρ_m, ρ_p, β_m, β_p, η, r and v correspond to pressure amplitude, particle volume, ultrasonic wavelength, wave vector, distance from a pressure node, density of the medium, density of particles, compressibility of medium, compressibility of particles, medium viscosity, particle radius, and relative velocity, respectively. In the experiments, all particles were of the same density and compressibility, but were different in size. Due to the fact that the acoustic force is proportional to the volume (r^3) of the particles, while the viscous force is proportional to the radius of the particles (r), larger particles experience much larger net forces and therefore move towards the pressure node faster than smaller ones.

When the channel width covers half a SSAW wavelength with a single pressure node at its center, dissimilar particles flowing along the sidewalls of the channel will be displaced towards the channel center by dissimilar net forces: the larger the particle, the larger the net force. Thus the particles are repositioned with different lateral displacements along the cross-section of the channel, which is split into multiple collection outlets. The collected sample is thus separated based on particle size, density, and compressibility. The minimum size difference between particles that is necessary for effective separation can be adjusted by tuning the SAW power and wavelength, the channel length, and the sample flow speed.

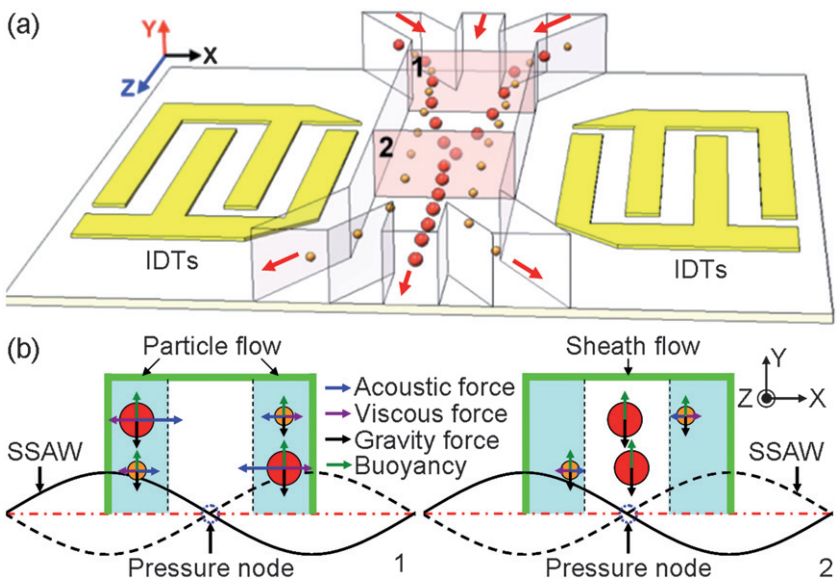

Fig. 1 (a) Schematic of the separation mechanism showing particles beginning to translate from the sidewall to the center of the channel due to axial acoustic forces applied to the particles when they enter the working region of the SSAW (site 1). The differing acoustic forces cause differing displacements, repositioning larger particles closer to the channel center and smaller particles farther from the center (site 2). (b) Comparison of forces (normally in pN range) acting on particles at site 1 and site 2, respectively.

Device fabrication and system setup

To achieve SAW with a high coupling coefficient, a Y + 128° X-propagation lithium niobate ($LiNbO_3$) wafer (500 μm thick) was used as the substrate for IDT deposition. The $LiNbO_3$ wafer was patterned with photoresist (SPR3012, MicroChem, Newton, MA), a double metal layer (Cr/Au, 50 Å/800 Å) was deposited (e-beam evaporator, Semicore Corp) on the wafer, and a lift-off process was used to remove the photoresist and the metal attached, thus obtaining the IDTs for SAW generation (Fig. 2(a)). A PDMS microchannel was then fabricated through a standard soft-lithograph and mold-replica procedure (Fig. 2(b)), and inlets/outlets were created using a silicon carbide drill bit. Lastly, the PDMS channel was properly aligned and bonded with the SAW substrate. In the bonding process, the bonding surfaces on both the PDMS channel and the SAW substrate were activated with oxygen plasma (50 sccm, 750 mTorr, 150 W, 2 min). A drop of ethanol was placed between the device substrate and the PDMS channel to act as a lubricant, permitting the channel to slide on top of the substrate until proper alignment was achieved. The partially bonded device was then put inside a vacuum chamber (50 °C, ~15 min) to remove the ethanol and enhance the bonding (more detailed information regarding the device fabrication can be found in ref. 29). An optical image of the final device is shown in Fig. 2(c). The width and pitch of the IDTs were 75 μm and 150 μm, respectively, corresponding to a SAW with a working wavelength of 300 μm. The PDMS channel is 150 μm in width and 80 μm in depth.

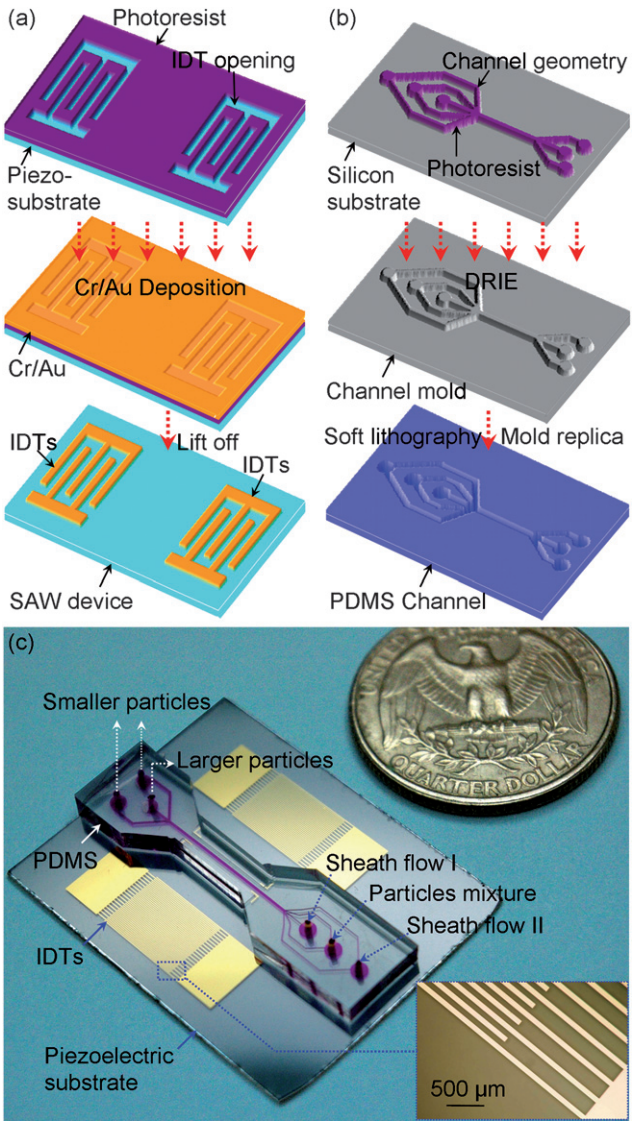

Fig. 2 (a, b) Schematic of the fabrication process and (c) optical image of the fabricated device. (a) A metal deposition (Cr/Au) followed by a lift-off process forming the IDTs on a piezoelectric substrate for SAW generation. (b) A mold-replica and soft-lithograph process forming the PDMS microchannel. (c) Optical image of the device used in the experiments, showing the inlets, outlets and zoom-in figure of the IDTs (inset).

The experiment was conducted on the stage of an inverted microscope (Nikon TE2000U). A mixture solution of fluorescent polystyrene beads (Particle I: 4.17 μm diameter, dragon green, ~2.53×10^7 beads/ml; Particle II: 0.87 μm diameter, Rhodamine WT, 2.76×10^8 beads/ml; both from Bangs Laboratories) was injected through the middle inlet, as shown in Fig. 2(c). DI water was injected through the inlets labeled sheath flow I and sheath flow II in Fig. 2(c). The central sheath flow separated the two particle streams, and the outer sheath flow prevented particles from trapping and aggregating along the sidewall of the channel due to surface roughness.[44] All three flows were injected using syringe pumps (KDS210, KD Scientific). Thus, a five-layer sandwiched laminar flow was formed across the channel (layer one: 1/2 sheath flow II; layer two: 1/2 particle flow; layer three: sheath flow I; layer four: 1/2 particle flow; layer five: 1/2 sheath flow II). An AC signal generated by an RF signal generator (Agilent E4422B) was amplified with a power amplifier (Amplifier Research 100A250A) and split into two signals, which were then applied to the two IDTs to generate two identical SAWs. The signal frequency was set at 12.6 MHz (resonance frequency of a SAW on $LiNbO_3$ at $\lambda = 300$ μm). Following that, the applied power (15–22 dBm, or 30–160 mW) and flow speed of the particle solution (0.6–2 μl/min) were tuned to achieve high separation efficiency. After passing through the microchannel, the particle solutions were collected at the outlets for quantitative analysis.

Results and discussions

Particle separation process

Two rectangular openings in the PDMS were fabricated on either side of the channel to define the working region of the SSAW. They also reduce the amount of PDMS in contact with the substrate, thus reducing propagation loss of the SAWs. Three positions marked as I, II and III along the channel were chosen to record the particle distribution in the channel when the SSAW was applied (Fig. 3(a)). At site I, particle flows and the sheath flow were entering the main channel. At this location, the particle mixture was outside of the working region of the SSAW, and small particles (red color) and large particles (green color) were flowing together along the sidewalls of the channel (Fig. 3(b)). Note that in site I the large particles are distributed in thin streams near the channel sidewall while the small particles form wider streams in the lateral direction of the channel; this is attributable to the hydrodynamic effect within the laminar flows.

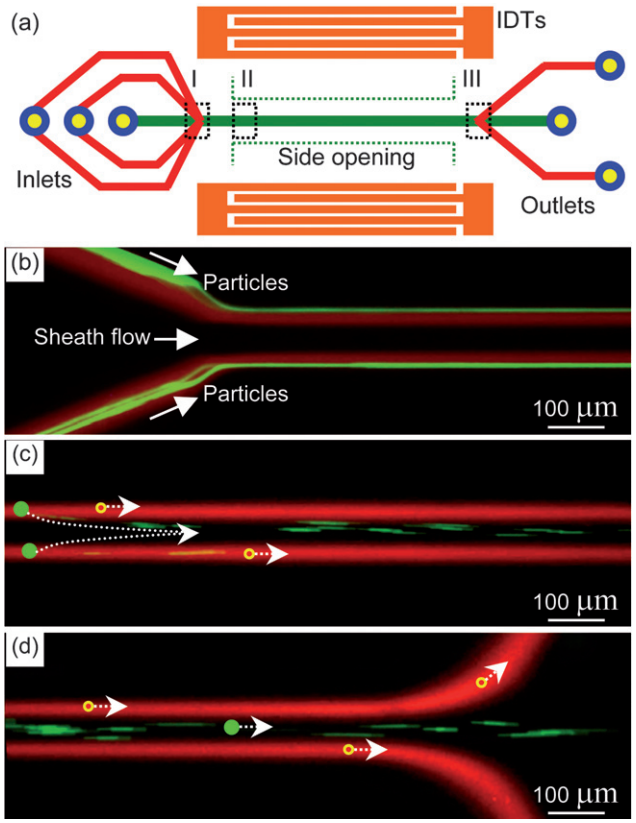

Fig. 3 (a) The schematic indicates the positions of the monitoring sites (I–III) for particle separation. (b)–(d) are the recorded fluorescent images at sites (I–III), respectively. Excitation light: 550 nm for 0.87 μm beads (with Rhodamine WT), and 480 nm for 4.16 μm beads (with dragon green). Fluorescent light: 590 nm for Rhodamine and 520 nm for dragon green. Each image shown in (b)–(d) is a composite of two images taken at the same position with different excitation light but the same working parameters.

As the particle mixture entered the working region of the SSAW (site II), the acoustic forces acting on the large particles were greater than those acting on the small particles, pushing the large particles out of the particle mixture and towards the SSAW pressure node at the center of the channel. The acoustic forces acting on the small particles were insufficient to push them into the central stream; thus the small particles remained in the side streams (Fig. 3(c)). As the large particles approached the SSAW pressure node, the acoustic forces acting on those particles decreased to zero, ensuring that the large particles remained in the central stream. An examination of Fig. 3(c) indicates that the large particles migrated to the central channel within a span of ~900 μm. Taking into account the flow speed (2.5 mm/s) of the particle flows, it is determined that the particle separation process took ~360 ms. It should be noted that by tuning the working parameters (increasing the flow speed and applied power), this separation time can be decreased further. At the outlet of the channel (site III), the large particles in the central stream were collected by the central outlet and the small particles in the two side streams were collected by the side outlets. At this point the particles were successfully separated (Fig. 3(d)). The similar size/density between cells and the microbeads used in our experiments indicate that this SSAW-based separation technology can be readily adopted in the separation of biological objects (*e.g.* cells).[36,38]

Separation efficiency analysis

To quantitatively evaluate the separation efficiency of this method, the particle samples collected from the side and central outlets were analyzed for size distribution. ImageJ® software was used to count the number of particles collected from each outlet. The remaining rate (the ratio of particles remaining in the side channel after SSAW exposure to the particles prior to SSAW exposure) and separation efficiency (the ratio of particles in the central channel after SSAW exposure to the particles prior to SSAW exposure) are shown in Fig. 4(a) and 4(b). While ~90% of the small particles remained in the side flows, more than 80% of the large particles migrated to the central flow. This high separation efficiency would yield noteworthy accuracy in sample detection and analysis, making this method attractive for a variety of bio/chemistry applications where experimental performance is highly dependent on the purity of samples (*e.g.*, microarrays, drug screening and regeneration, and tissue engineering).[45–50]

Theoretical analysis

When a microparticle maintains constant velocity in the SSAW field, the acoustic and viscous forces balance each other.[36,51] Based on eqn (1)–(3), we conclude

$$v_h = -[p_0^2 V_c \beta_w/(12\lambda\eta r_c)]\phi(\rho,\beta)\sin(4\pi x/\lambda). \quad (4)$$

Rewriting $v_h = -dx/dt$ and separating variables, we obtain:

$$\cos ec(4\pi x/\lambda)dx = [p_0^2 V_c \beta_w/(12\lambda\eta r_c)]\phi(\rho,\beta)dt \quad (5)$$

Since the particles will move to the pressure nodes nearby, δx is in the range of (0, $\lambda/4$). Therefore the time needed for bead migration will be

$$t = (3\lambda^2\eta r_c/\pi)[\ln(\tan(2\pi x/\lambda))]^{x_2}_{x_1}/[p_0^2 V_c \beta_w \phi(\rho,\beta)] \quad (6)$$

where x_1 and x_2 are the starting and ending positions in the lateral direction (x axis). The above mathematical expressions can be used to predict the SSAW-induced flow paths of particles with different properties (size, density and compressibility). This

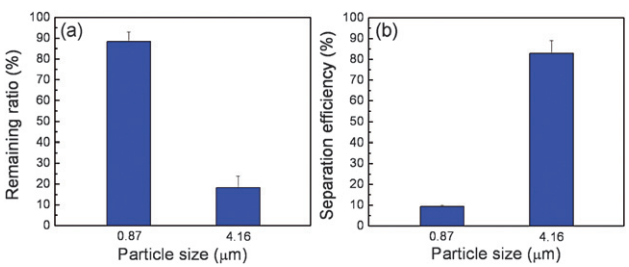

Fig. 4 Quantitative analysis showing (a) the ratio of particles remaining in the side channel (remaining rate) after passing through the SSAW working region, and (b) the ratio of particles in the central channel (separation efficiency) after passing through the SSAW working region.

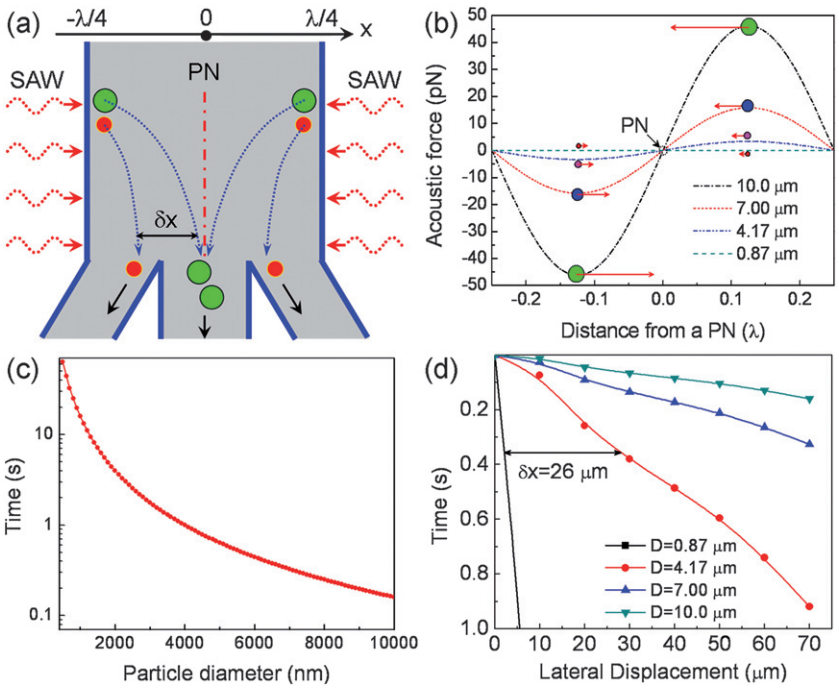

Fig. 5 (a) The schematic for the model used in calculation: parallel flowing particles along the sidewall of the channel experience lateral acoustic forces and translate through different lateral displacements (δx), resulting in the separation. (b) Primary acoustic force distribution along a SSAW wavelength. (c) Time required for particles with varying sizes to translate from the sidewall of the channel to the pressure node at the center. (d) Relative lateral displacement (along x axis) *versus* the working time of SSAW.

prediction of particle flow paths enables optimization of the channel design and SAW working parameters.

In a simplified model (Fig. 5(a)), particles of two different sizes but otherwise identical properties enter the working region of the SSAW along the sidewall of the channel. Due to the difference in magnitude of the acoustic forces acting on the particles (Fig. 5(b)), the larger particle reaches the pressure node at the center of the channel in less time than does the smaller particle (Fig. 5(c)). Fig. 5(d) plots the lateral displacements of particles (polystyrene beads) of different sizes *versus* time of SSAW exposure, where the relative distance δx between the particles used in the experiment (0.87 μm and 4.17 μm polystyrene beads) was calculated to be ~26 μm in 360 ms, which coincides well with the experimental result observed in Fig. 3(c).

Conclusions

By introducing a SSAW in a microfluidic channel, particles of varying sizes can be effectively and continuously separated. The excellent energy-confinement of SAWs propagating on a piezoelectric substrate makes this particle separation device highly energy efficient: 13,000 particles were separated from a dissimilar mixture in one minute using 30 mW of power, notably smaller than the 500–2000 mW required by BAW-based acoustophoresis in an equivalent situation.[27,28] In addition, while the BAW-based method requires the channel material to possess excellent acoustic reflection properties (*e.g.*, silicon, glass, *etc.*), this SSAW-based approach confines the acoustic wave to the substrate, permitting the use of convenient channel materials such as PDMS. This particle separation device is fabricated *via* standard MEMS and soft-lithography procedures, permitting easy fabrication, miniaturization, and integration—and making it highly cost-effective for potential mass production. Furthermore, the separation efficiency of this technique (~80%) is comparable to or higher than the efficiencies of other techniques. And the separation efficiency and speed of this technique can be readily adjusted by tuning applied SAW power, working wavelength of the SAWs, sample flow speed, and channel geometry. These characteristics make the SSAW-based particle separation method presented here promising in many bio/chemical applications.

Acknowledgements

We thank Xiaole Mao and Sz-Chin Steven Lin for helpful discussion. This research was supported by National Science Foundation (ECCS-0824183 and ECCS-0801922) and the Penn State Center for Nanoscale Science (MRSEC). Components of this work were conducted at the Penn State node of the NSF-funded National Nanotechnology Infrastructure Network.

Notes and references

1 C. W. Yung, J. Fiering, A. J. Mueller and D. E. Ingber, *Lab Chip*, 2009, **9**, 1171–1177.
2 O. Lara, X. Tong, M. Zborowski and J. J. Chalmers, *Exp. Hematol.*, 2004, **32**, 891–904.
3 N. Ye, J. Qin, W. Shi, X. Liu and B. Lin, *Lab Chip*, 2007, **7**, 1696–1704.
4 P. O. Krutzik, J. M. Crane, M. R. Clutter and G. P. Nolan, *Nat. Chem. Biol.*, 2008, **4**, 132–142.
5 J. Seo, M. H. Lean and A. Kole, *Appl. Phys. Lett.*, 2007, **91**, 033901.
6 N. Pamme, *Lab Chip*, 2007, **7**, 1644–1659.
7 C. Blattert, R. Jurischka, A. Schoth, P. Kerth and W. Menz, *Proc. SPIE–Int. Soc. Opt. Eng.*, 2004, **5345**, 17–25.

8 B. Qu, Z. Wu, F. Fang, Z. Bai, D. Yang and S. Xu, *Anal. Bioanal. Chem.*, 2008, **392**, 1317–1324.
9 K. McCloskey, J. Chalmers and M. Zborowski, *Anal. Chem.*, 2003, **75**, 6868–6874.
10 M. Yamada, M. Nakashima and M. Seki, *Anal. Chem.*, 2004, **76**, 5465–5471.
11 A. A. S. Bhagat, S. S. Kuntaegowdanahalli and I. Papautsky, *Lab Chip*, 2008, **8**, 1906–1914.
12 A. A. S. Bhagat, S. S. Kuntaegowdanahalli and I. Papautsky, *Phys. Fluids*, 2008, **20**, 101702.
13 L. R. Huang, E. C. Cox, R. H. Austin and J. C. Sturm, *Science*, 2004, **304**, 987–990.
14 J. Takagi, M. Yamada, M. Yasuda and M. Seki, *Lab Chip*, 2005, **5**, 778–784.
15 D. H. Yoon, J. B. Ha, Y. K. Bahk, T. Arakawa, S. Shoji and J. S. Go, *Lab Chip*, 2009, **9**, 87–90.
16 J. P. Beech and J. O. Tegenfeldt, *Lab Chip*, 2008, **8**, 657–659.
17 L. C. Jellema, T. Mey, S. Koster and E. Verpoorte, *Lab Chip*, 2009, **9**, 1914–1925.
18 S. Choi and J.-K. Park, *Lab Chip*, 2009, **9**, 1962–1965.
19 Z. Wu, B. Willing, J. Bjerketorp, J. K. Jansson and K. Hjort, *Lab Chip*, 2009, **9**, 1193–1199.
20 J.-C. Baret, O. J. Miller, V. Taly, M. Ryckelynck, A. El-Harrak, L. Frenz, C. Rick, M. L. Samuels, J. B. Hutchison, J. J. Agresti, D. R. Link, D. A. Weitz and A. D. Griffiths, *Lab Chip*, 2009, **9**, 1850–1858.
21 S. Zhao, H. Cong and T. Pan, *Lab Chip*, 2009, **9**, 1128–1132.
22 I. Doh and Y. Cho, *Sens. Actuators, A*, 2005, **121**, 59–65.
23 B. G. Hawkins, A. E. Smith, Y. A. Syed and B. J. Kirby, *Anal. Chem.*, 2007, **79**, 7291–7300.
24 T. Braschler, N. Demierre, E. Nascimento, T. Silva, A. G. Oliva and P. Renaud, *Lab Chip*, 2008, **8**, 280–286.
25 M. Abdelgawad, M. W. L. Watson and A. R. Wheeler, *Lab Chip*, 2009, **9**, 1046–1051.
26 H.-H. Cui, J. Voldman, X.-F. He and K.-M. Lim, *Lab Chip*, 2009, **9**, 2306–2312.
27 F. Perterson, A. Nilsson, C. Holm, H. Jönsson and T. Laurell, *Analyst*, 2004, **129**, 938–943.
28 F. Petersson, L. Aberg, A. Swärd-Nilsson and T. Laurell, *Anal. Chem.*, 2007, **79**, 5117–5123.
29 Y. N. Xia and G. M. Whitesides, *Annu. Rev. Mater. Sci.*, 1998, **28**, 153–184.
30 D. Ahmed, X. Mao, J. Shi, B. K. Juluri and T. J. Huang, *Lab Chip*, 2009, **9**, 2738–2741.
31 C. Campbell and J. C. Burgess, *J. Acoust. Soc. Am.*, 1991, **89**, 1479–1480.
32 Z. Guttenberg, H. Müller, H. Habermüller, A. Geisbauer, J. Pipper, J. Felbel, M. Kielpinski, J. Scriba and A. Wixforth, *Lab Chip*, 2005, **5**, 308–317.
33 M. K. Tan, J. R. Friend and L. Y. Yeo, *Lab Chip*, 2007, **7**, 618–625.
34 A. Wixforth, C. Strobl, C. Gauer, A. Toegl, J. Scriba and Z. V. Guttenberg, *Anal. Bioanal. Chem.*, 2004, **379**, 982–991.
35 T. Frommelt, M. Kostur, M. Wenzel-Schafer, P. Talkner, Peter Hanggi and A. Wixforth, *Phys. Rev. Lett.*, 2008, **100**, 034502.
36 J. Shi, D. Ahmed, X. Mao, S. S. Lin, A. Lawit and T. J. Huang, *Lab Chip*, 2009, **9**, 2890–2895.
37 H. Li, J. R. Friend and L. Y. Yeo, *Biomed. Microdevices*, 2007, **9**, 647–656.
38 J. Shi, X. Mao, D. Ahmed, A. Colletti and T. J. Huang, *Lab Chip*, 2008, **8**, 221–223.
39 T. Franke, A. R. Abate, D. A. Weitz and A. Wixforth, *Lab Chip*, 2009, **9**, 2625–2627.
40 M. Hennig, J. Neumann, A. Wixforth, J. O. Rädler and M. F. Schneider, *Lab Chip*, 2009, DOI: 10.1039/b907157a.
41 K. Sritharan, C. J. Strobl, M. F. Schneider and A. Wixforth, *Appl. Phys. Lett.*, 2006, **88**, 054102.
42 K. Yosioka and Y. Kawasima, *Acustica*, 1955, **5**, 167–173.
43 A. Nilsson, F. Petersson, H. Jönsson and T. Laurell, *Lab Chip*, 2004, **4**, 131–135.
44 M. I. Lapsley, S. S. Lin, X. Mao and T. J. Huang, *Appl. Phys. Lett.*, 2009, **95**, 083507.
45 C. J. Flaim, S. Chien and S. N. Bhatia, *Nat. Methods*, 2005, **2**, 119–125.
46 D. B. Wheeler, A. E. Carpenter and D. M. Sabatini, *Nat. Genet.*, 2005, **37**, S25–S30.
47 M. M. Stevens, M. Mayer, D. G. Anderson, D. B. Weibel, G. M. Whitesides and R. Langer, *Biomaterials*, 2005, **26**, 7636–7641.
48 V. K. S. Hsiao, J. R. Waldeisen, Y. B. Zheng, P. F. Lloyd, T. J. Bunning and T. J. Huang, *J. Mater. Chem.*, 2007, **17**, 4896–4901.
49 T. J. Huang, M. Liu, L. D. Knight, W. W. Grody, J. F. Miller and C.-M. Ho, *Nucleic Acids Res.*, 2002, **30**, e55.
50 S. R. Khetani and S. N. Bhatia, *Nat. Biotechnol.*, 2008, **26**, 120–126.
51 R. K. Gould and W. T. Coakley, *Proceedings of the 1973 symposium on Finite Amplitude Wave Effects in Fluids*, 1974, 252–257.